PROBABILISTIC MODEL OF LASER RANGE FINDER FOR THREE DIMENSIONAL GRID CELL IN CLOSE RANGE ENVIRONMENT

Hafiz Iman and Nahrul Khair Alang Md Rashid

Department of Mechatronics Engineering,
Faculty of Engineering, International Islamic University Malaysia,
Jalan Gombak, 53100, Kuala Lumpur, Malaysia.

hafiz.ghazman@gmail.com, and nahrul@iium.edu.my

ABSTRACT: The probabilistic model of a laser scanner presents an important aspect for simultaneous localization and map-building (SLAM). However, the characteristic of the beam of the laser range finder under extreme incident angles approaching 90^0 has not been thoroughly investigated. This research paper reports the characteristic of the density of the range value coming from a laser range finder under close range circumstances where the laser is imposed with a high incident angle. The laser was placed in a controlled environment consisting of walls at a close range and 1000 iteration of scans was collected. The assumption of normal density of the metrical data collapses when the beam traverses across sharp edges in this environment. The data collected also shows multimodal density at instances where the range has discontinuity. The standard deviation of the laser range finder is reported to average at 10.54 mm, with 0.96 of accuracy. This significance suggests that under extreme incident angles, a laser range finder reading behaves differently compared to normal distribution. The use of this information is crucial for SLAM activity in enclosed environments such as inside piping grid or other cluttered environments.

ABSTRAK: Model berkebarangkalian pengimbas laser membentangkan aspek penting untuk pemetaan dan penganggaran lokasi (SLAM). Walau bagaimanapun, sifat pancaran laser pada sudut pantulan menghampiri 90^0 masih belum dikenalpasti dan tidak dikaji secara mendalam. Oleh itu, kertas penyelidikan inibertujuan untuk melaporkan sifat taburan normal yang datang dari pengukur jarak laser di bawah keadaan jarak dekat di mana laser itu dikenakan dengan sudut insiden tinggi. Pengimbas laser diletakkan di tempatterkawal yang terdiri daripada muka diding pada jarak yang dekat dan 1000 imbasan dikumpulkan. Andaian ketumpatan normal data berhubung dengan jarak ukuran runtuh apabila pantulan laser merentasi sudut tajam dalam tempat terkawal. Data yang dikumpul juga menunjukkan kepadatan pasca-modal pada keadaan di mana julat mempunyai ketakselanjaran. Sisihan purata taraf pengukur jarak laser dilaporkan berpurata pada 10.54 mm di bawah ketepatan 0.96. Penemuan menunjukkan bacaan pengimbas laser tidak mempunyai sifat taburan normal.Pengetahuan ini wajar digunakan untuk SLAM di kawasan yang tertutup rapat seperti di dalam grid pempaipan dan persekitaran yang berselerak.

1. INTRODUCTION

Simultaneous localization and mapping (SLAM) requires a robust sensor with known and tested measurement model. In regard to the theme of mapping an environment

probabilistically using continuous density, the model of a laser range finder is crucial for an esteem map. A laser range finder is an active range-bearing sensor that produces bearing information and range measurement collectively known as metrical data. While transmitting and receiving beam reflection, the light source of a laser range finder is reflected by a right-angled mirror or prism depending on the model of the laser scanner. The mirror is mounted on a built-in turntable and rotates about the z-axis.

In Fig. 1, the sequence of the rotation is shown to start at $t_{initial}$ and move in a circular fashion to t_{final}, known as planar sweeping.
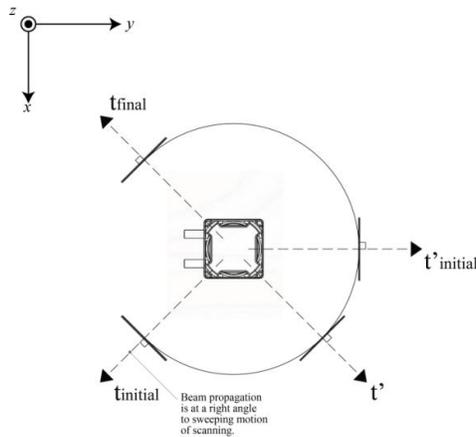
Fig. 1: The sequence of a laser range finder, in the case of this paper the Hokuyo UTM-30LX, that has an active region of 270^0, doing a planar sweep to gather continuous stream of metrical data.

The beam propagation is perpendicular to the direction of the circular motion, and with continuous data acquisition, the beam will produce a metrical data as shown in Fig. 2. Figure 2 depicts three dimensional point clouds consisting of multiple layers of metrical data obtained from planar sweeping. The geometric information in point clouds are noise ridden and discontinuous which pose challenges to researchers.
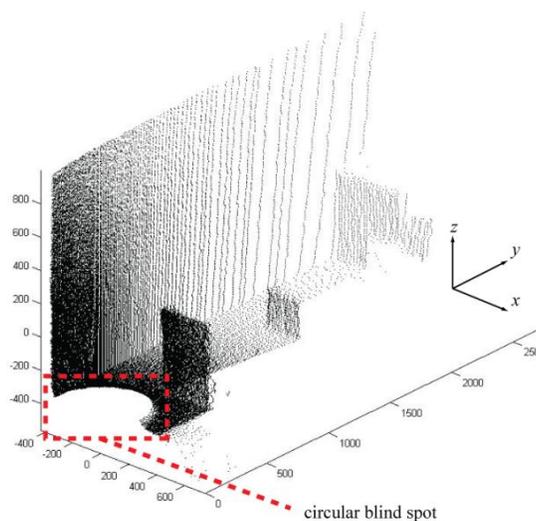
Fig. 2: The metrical data, which is planar in nature, can be extended to spatial representation known as point clouds.

Without the model of the laser range finder, any SLAM solution would risk incorporating error in the measurement data. The need for the model proves more crucial since the sensor produces predominant noise in a confined-close-range environment due to bounce and beam width [1]. To remedy the uncertainty of the reading, the sensor should be modeled probabilistically [2]. However, attempts to quantify the parameter of a normal distribution for any laser range finder's reading using density estimation method has yet to be introduced in the literature. Furthermore, the Gaussian modality of density of a laser range finder reading for close range confined space in a static environment has not been documented.

Density estimation is a statistical method to objectively select suitable pattern of random variables without the assumption that these variables belong to any distribution. This method eliminates any pre-assumption of distribution eliminating bias density. The method underlines a smoothing algorithm based on a certain bandwidth. Although Kernel density estimation regarded as trivial to some researchers, this paper will be attempting to use such method to investigate the density of the metrical data obtained by a laser range finder. The result of the density estimation method will also be used to determine if the modality of the metrical data can be represented by unimodal distribution under close range confined space.

The efforts to prove that laser range finder readings follow Gaussian density are crucial because the parameters from the density would give an insight, as an example, to an appropriate selection of a SLAM solution. With known value of probability parameter, the characteristic on the modality and accuracy of the sensor can be described succinctly [3]. The value can be used to optimize the SLAM solution and to indicate the type of filtering technique suitable for any adopted SLAM solution. The standard deviation of the sensor can also be used to pre-compute and approximate the Gaussian of the sensor measurement without having to iterate the Gaussian function each time a measurement is collected [4]. In this paper, kernel density estimation is used to compute the standard deviation of Hokuyo UTM-30LX under close range environment. Figure 3 explains the process of obtaining the probability parameter from metrical data collected by the laser scanner.
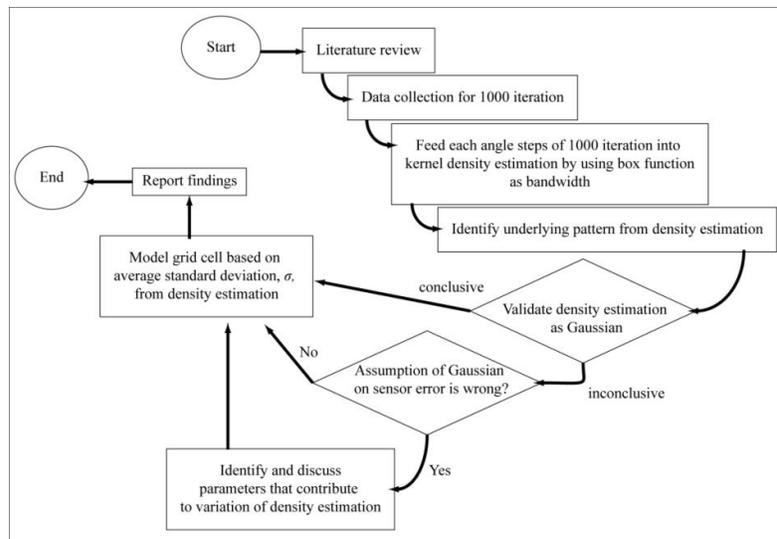
Fig. 3: Workflow for density estimation for a laser range finder called Hokuyo UTM-30LX.

Literature review guides the procedural aspect of this paper on how to obtain and gestate data from scanning sensor such as Hokuyo UTM-30LX. The literature review is followed by data collection using the scanner and feeding this data into kernel density estimation method. The underlying pattern present by the data via kernel density method would be used to validate the nature of the density obtained from metrical data collected by UTM-30LX under confined close range space. The pattern, in a form of density, is also used to find the standard deviation of the laser scanner. Upon conclusion of the most optimized value of standard deviation, the model grid cell of the sensor and the occlusion in close range space can be modeled.

2. RELATED WORK

Ye and Borenstein [5] outlined a method to characterize a laser scanner by imposing the scanner with various angles of reflection and collected multiple data series under such condition. Fig. 4 shows the setup of their experiment, configured to impose varying angle of incident to one particular beam at a time. The laser scanner was mounted on a linear motion table where the distance of target and laser scanner could be varied, and the target surface was mounted on a rotatable stage for varying angle of eflection. The turn table is used to change the incident angle and a linear table was used to change the range between the target, placed on the turn table, and the scanner.
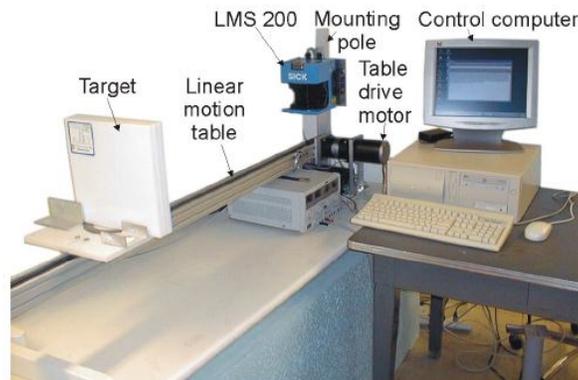
Fig. 4: The experimental setup for parametric investigation of LMS 200 LIDAR by
Ye and Borenstein [5].

Ye and Borenstein [5] assimilate their method by using SICK LMS-200. Their method was reiterated by a number of researchers including Kneip et al. [6] that uses Hokuyo URG-04LX 2D laser scanner. Both lasers, SICK LMS-200 and Hokuyo URG-04LX, are based on the principle of time of flight (TOF) validating that the method used by Ye and Borenstein [5] is applicable for Hokuyo URG-04LX. However, [6] extend the method by subjecting the laser scanner with different type of surface during scanning. Their report concluded that the angle of reflection has marginal effect on the accuracy and of the sensor reading. They also concluded that the laser produces marginal error for different surfaces,. However, Kneip et al. [6] suggest that Hokuyo URG-04LX application should be confined to an environment that has minimal number of transparent or highly reflective surfaces. The lack of performance due to reflective and transparent surface is amplified, Alwan et al. [7]. They reported that due to the nature of the source of a laser scanner, which is an amplified electromagnetic wave, light based LIDAR such as PBS 03JN, Hokuyo UTM-30LX, and SICK LMS-200 would register erroneous metrical data. This is because the reaction of light,

or lack thereof, to transparent surface would produce a bias maximum reading. Also, the light beam would bounce at a wider beam width if a reflective surface is present which contributes to the bias reading.

One aspect of map-building for autonomous robot is the selection of LIDAR or laser scanner. Hokuyo laser scanners for example cater the need of autonomous robotics by producing a family of laser scanners that has a desirable weight to range ratio. Figure 5 identifies laser scanners based on their weight and maximum range [8]. It is observed that two of the Hokuyo laser scanner, URG-04LX and UBG 04LX, have a light weight feature but with maximum range of less than 10 meters. In spite of this shortcoming, the newest generation of Hokuyo laser scanner, the UTM-30LX, has a range of 30 m which weighs within 1 kg. The scanner is considerably light weight for a capacity of 30 m which rivals the more expensive laser scanner such as SICK LMS-200. It is evident that the ratio of maximum range to weight of UTM-30LX is the highest among all laser scanners as seen in Figure 5. This motivates the use of Hokuyo UTM-30LX in this research paper.
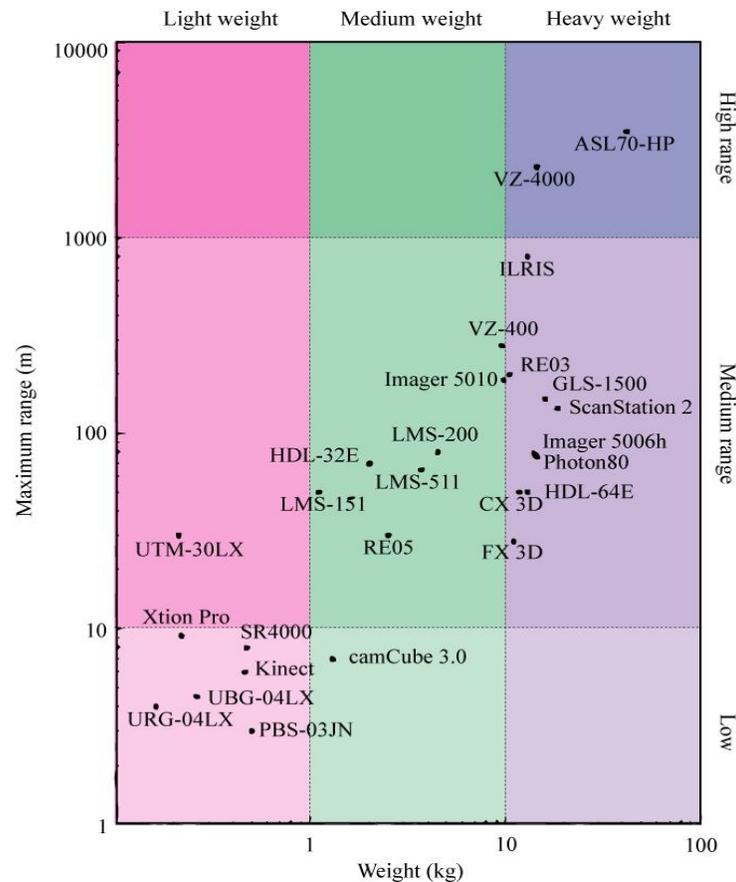
Fig. 5: Mapping of various scanner models based on their weights and maximum range of scannings [8].

The characterization of the Hokuyo laser scanner particularly UTM-30LX, which will be used in this paper, has been limited. Demski et al. [9] have produced results of their experiment based on Ye and Borenstein [5] method using Hokuyo UTM-30LX. Demski et al. [9] suggested that the performance of Hokuyo UTM-30LX was under the standard deviation of 5 mm. Their report acknowledged the drift of the laser scanner reading if the

scanning period was prolonged to two hours and more. The drift was also reported by Pouliot et al. [10] who use the same Hokuyo UTM-30LX for their power line inspection robot called LineScout. The standard deviation reported by Pouliot et al. [10] was between 4.8 mm to 6.3 mm. The standard deviation of both Demski et al. [9] and Pouliot et al. [10] however, are assumed statistically without knowing the modality of the error's probability. Another work that characterize the error of Hokuyo laser are by Park et al. [11] who used UBG 04LX that follows the guidelines elucidated by Ye and Borenstein [5]. Tretyakov and Linden [12] evaluated the performance of UTM-30LX together with other scanners namely, SICK's LMS-291 and LMS-III, Swiss Ranger MESA SR-3100, and Microsoft Kinect under smoky condition. Tretyakov and Linden [12] validate the accuracy performance of the aforementioned scanners when introduced within a smoke laden room. The performance benchmark of the scanners is based on the absorbability of the transmission signal of all the scanners. The paper uses extinction coefficient to quantify the energy loss of the signal due to absorbability. All scanners performed well in smoky environment with mention of stellar performance by Microsoft Kinect and SICK LMS-291.

Thus far, all the literatures discussed have performed characterisation of laser scanners under ambient lighting. Pomerleau et al. [8] raises the issue of laser scanner performance under direct sunlight and in highly reflective environment. Much of the procedure was based on Ye &Borenstein[5] that uses three different laser scanners; SICK LMS-151, Hokuyo URG-04LX and UTM-30LX. The standard deviation of the sensor was reported to be 28 mm for URG-04LX, 18 mm for UTM-30LX, and 12 mm for LMS-151. These standard deviations are excerpts from a histogram method. The approach also assumes single modality of the entire scanner's error.

3. GRID CELL OF LASER RANGE FINDER

In this paper, the probabilistic model of the Hokuyo UTM-30LX is hypothesized to be Gaussian. The Gaussian model will be used to compare the result of the kernel density estimation based on measurement collected. This paper will adopt a relaxed beam model, also known as ray tracing approach, based on the contingency that follows a close range confined space. The relaxed beam model is designed to reflect the assumptions that:

- the environment is static, having no transparent or near transparent structure i.e glass

- the geometric data of the environment are confined in a cube of width, depth, and length of less than 6000 mm

- the sensor reading is independent of the absolute location of the sensor per se

- the model of the sensor is prescribed before an actual grid map-building commence

The beam model consists of four terms of probability functions:

$$f_{total}(w_1, w_2, w_3, w_4) = w_1 f_{1:z,x_1,m} + w_2 f_{2:z,x_2,m} + w_3 f_{3:z,x_3,m} + w_4 f_{4:z,x_4,m} \tag{1}$$

$f_{n:z,x,m}$ represent constituent conditional probability function regarding aspect of a laser model where, z, represents observation or measurement reading of an occlusion; x, represents the state of an autonomous robot; m, represents the map of the environment; w_n, the weight of importance of the function term Thrun [2]. Since the model is based solely on the measurement of an occlusion, the function is simplified to,

$$f_{total}(w_1, w_2, w_3, w_4) = w_1 f_{1:z} + w_2 f_{2:z} + w_3 f_{3:z} + w_4 f_{4:z} \tag{2}$$

There are four terms in Eqn.(2) each models a contingent in the measurement of a scanner. $f_{1:z}$ represent the accuracy and the repeatability of the sensor and the footprint of the beam of the sensor:

$$f_{1:z}(z) = \left| \begin{array}{l} \dfrac{1}{\eta} N(z, \mu, \sigma^2) \quad \text{if} \quad z \in [0, z_{\max}] \\ 0 \quad \text{if} \quad z > z_{\max} \end{array} \right. \tag{3}$$

where z_{max} is the maximum range of the scanner; μ, is the median; σ^2, is the variance of the Gaussian and, η, is the normalizing factor for the Gaussian function N.

$f_{2:z}$ represents the probability of the scanner when it reached its maximum reading:

$$f_{2:z}(z) = \left| \begin{array}{l} step(z_{\max}) \quad \text{if} \quad z \in [0, z_{\max}] \\ 0 \quad \text{if} \quad z > z_{\max} \end{array} \right. \tag{4}$$

This occurs when there is no occlusion within the maximum range of the scanner.

$f_{3:z}$ represents interference of the scanner with other scanners and surface reflection of the propagating beam with surface of any angle: The value is inverse of z_{max} so that the total area of density $f_{3:z}$ is unity.

$$f_{3:z}(z) = \left| \begin{array}{l} \dfrac{1}{z_{\max}} \quad \text{if} \quad z \in [0, z_{\max}] \\ 0 \quad \text{if} \quad z > z_{\max} \end{array} \right. \tag{5}$$

f_4 represents the dynamic obstacle in the scanner active range which can be expressed as:

$$f_{4:z}(x) = \left| \begin{array}{l} \dfrac{1}{\eta} \lambda e^{-\alpha z} \quad \text{if} \quad z \in [0, z_{\max}] \\ 0 \quad \text{if} \quad z > z_{\max} \end{array} \right. \tag{6}$$

λ, and, α, represent coefficients chosen to reflect the degree of importance of the decaying aspect of the function. Decaying function is used to represent dynamic occlusion because the further the dynamic occlusion is from the scanner, the less probable that any object behind this dynamic occlusion have any effect on the measurement of the scanner. With all of the terms having a weight, w_n, of unity, Eqn.(1) can be depicted as shown in Fig. 6.
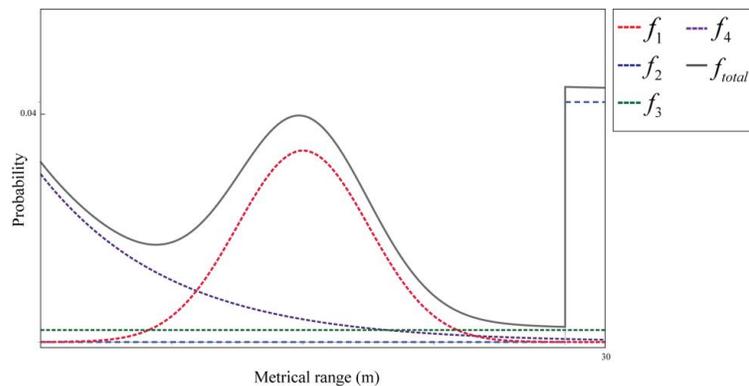
Fig. 6: The beam tracing model represented by f_{total}.

However, since the relaxed beam model is of concern in this paper, Eqn. (1) is rendered to,

$$f = f_{1:z} + f_{3:z}$$

(7)

Figure 7 depicts the shape of the probabilistic model of the scanner measurement.
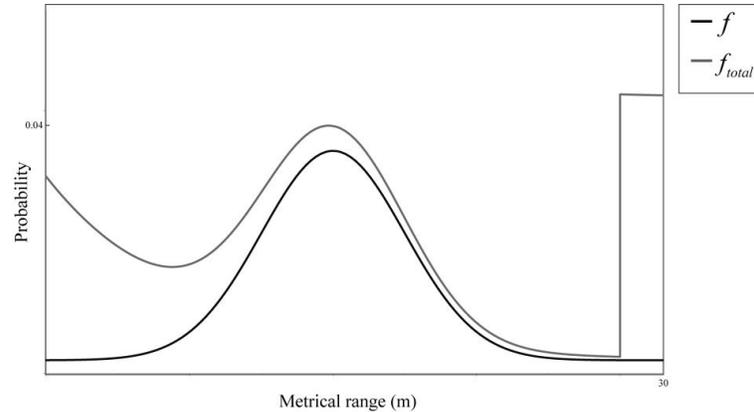
Fig. 7: Comparison between the beam tracing model, f_{total}, with the relaxed beam tracing model, f.

With the model of the relaxed beam tracing established, the underlying density of the metrical range data can be compared. The kernel estimation method is used to validate the modality of the metrical data coming from laser range finder without any pre-assumption that the measurements would be Gaussian. In this paper, the kernel density estimation method is done by minimizing the error between the underlying pattern and the random variables using box bandwidth as the kernel [13]. The method was derived from statistical method used to find optimal bin size for histogram for neuronal spike [14]. The method introduced in [13] and [14] are chosen because they do not assume any underlying pattern of the density of the reading. The absence of this assumption helps in investigating the actual distribution of the sensor reading under close range confined space because this method can eliminate any biased towards normal distribution if the readings are not Gaussian.

Seven different locations in the controlled environment are sampled. These seven locations will be represented by range, or depth, of the laser reading. These random variables are used to estimate the underlining pattern of the laser error characteristic by using kernel density estimation as mentioned above. It should be noted again that this method does not assume the error of the laser reading to be Gaussian to eliminate any bias towards normal distribution if the reading is multimodal or non-Gaussian. The resulting density will be used to validate whether the scanner can be modeled based on the relaxed beam model. Also, with the estimated density at hand, the most optimal standard deviation of the laser scanner can be found.

The purpose of finding standard deviation for the scanner is to model the grid cell that represents occlusion and reading error based on the reading of the scanner. Mentioned in the introduction of this paper was the importance of finding parameter of density of a sensor; to give insight to potential SLAM solution. Grid cell, a model of occlusions in space, is a part of the solution to SLAM. The standard deviation is used to extend the grid cell to three dimensions which follows the premise introduced by Pomerleau et al. [8]. Pomerleau et al. [8] selected the bigger value of standard deviation between the range uncertainty reading and the beam width to parameterize their isotropic model of sensor error. Pomerleau et al.

[8] also introduce anisotropic model of the sensor bounded by these two parameters; the standard deviation of the depth along the beam propagation and the standard deviation of the beam width, forming an ellipsoid depicted in Fig. 8. However, grid cell, in the form of cubes, used the knowledge of the sensor error parameter to model the sensor and the occlusion. By using a cube, the tessellation of the cubic grid cell will produce a continuous map. The dimension of the cube takes the value of 95% confidence of the scanner metrical range, *6*σ*. Figure 8 compares the structure of both the grid cell model of this paper and that of Pomerleau et al. [8].
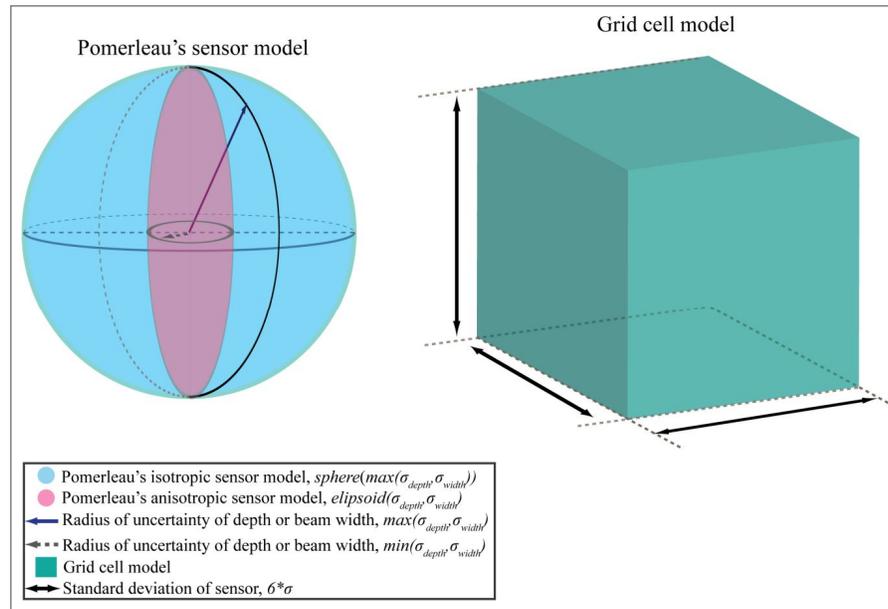
Fig. 8: Isotropic and anisotropic sensor models and the grid cell model adopted in this paper [8].

The method of tessellating the grid cell is beyond the scope of this paper but the grid cell would cluster the metrical data into voxel that has dimensions based on the value of the sensor's standard deviation. Figure 9 shows a sample of grid cell tessellation based on standard deviation of a scanner.

4. PROCEDURE PROTOCOL

In this paper, close-range environment is defined by a pronounced incident angle imposed to the sensor and the abrupt changes in the range of occlusion. Taking reference from few literatures such as the work of Ye and Borenstein [5], the experiment protocol consists of collecting range data in a controlled environment subjected to occlusions, in a form of walls, for 1000 iterations. With 1000 iterations, which produce 1000 scans, Gaussian estimation can be performed on each angle increment of planar sweeping. The range of the planar sweeping is limited between -2.25^0 to 182.25^0.

In Fig. 10, the sensor is place at a close range of 40 mm from the wall. At a very small clearance of 40 mm, large incident angle is imposed to the scanner which has the propagating beam centers at 30 mm off from the outside chassis. The position of the laser between the two corners is asymmetrical. The distance between the laser and the *first corner* is 2770 mm and the distance between the laser and the *second corner* is 5670 mm. The

asymmetric nature of the laser scanning field divides the planar sweeping into two areas. While both areas have high angle of incident for scanning activity, the first half of the planar sweeping area has a relatively lower incident angle than the second half of the planar sweeping.
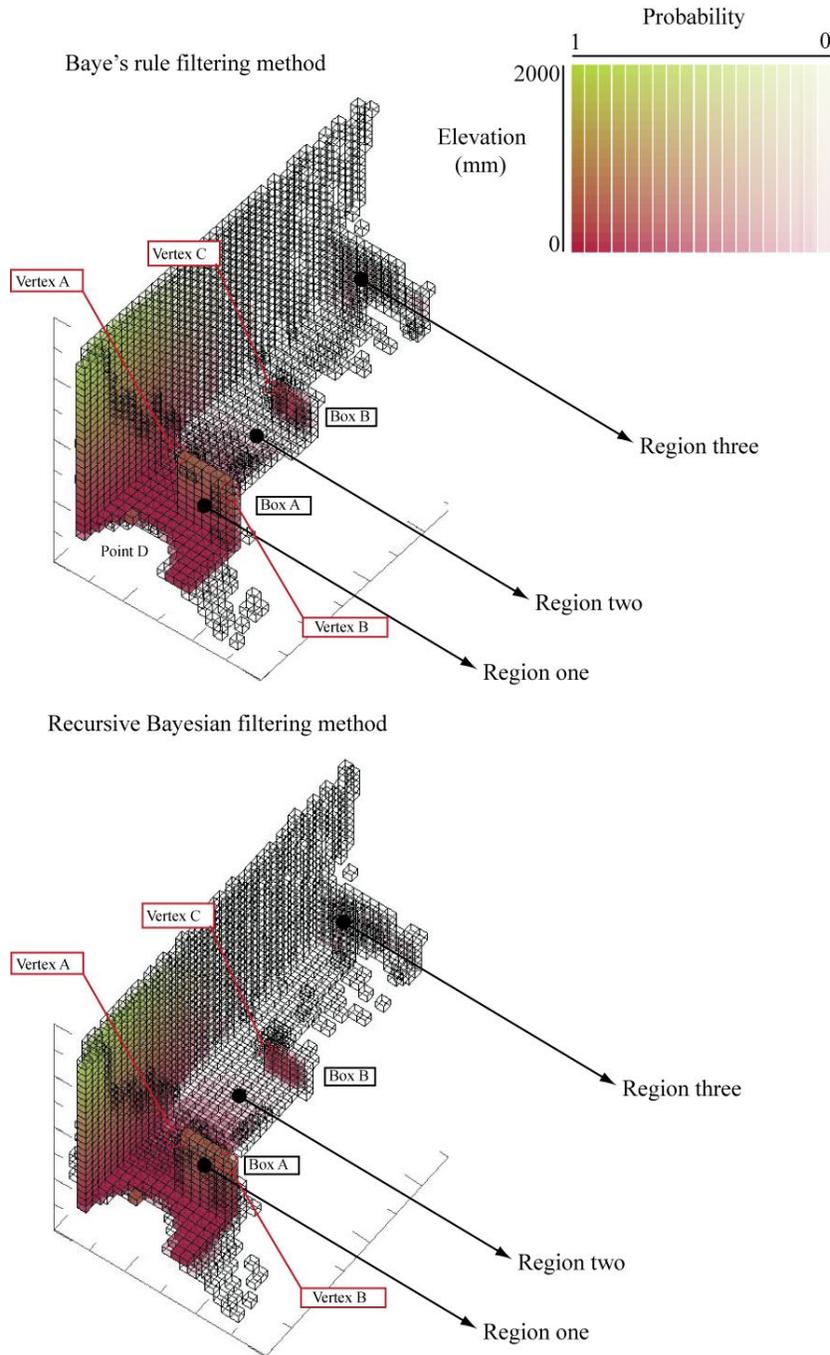
Fig. 9: An example of grid cells tessellation to produce continuous map optimized by Recursive Bayesian filtering method and Bayes' rule filtering method.

As mentioned above, the laser scanner would collect metrical data called metrical range that scatters along the line of propagation of the beam as shown in Fig. 11. Since Hokuyo UTM-30LX has the maximum range of 30 m, the metrical range data would produce a *faux* range reading of 30 m if there is no occlusion within the 30 m range.
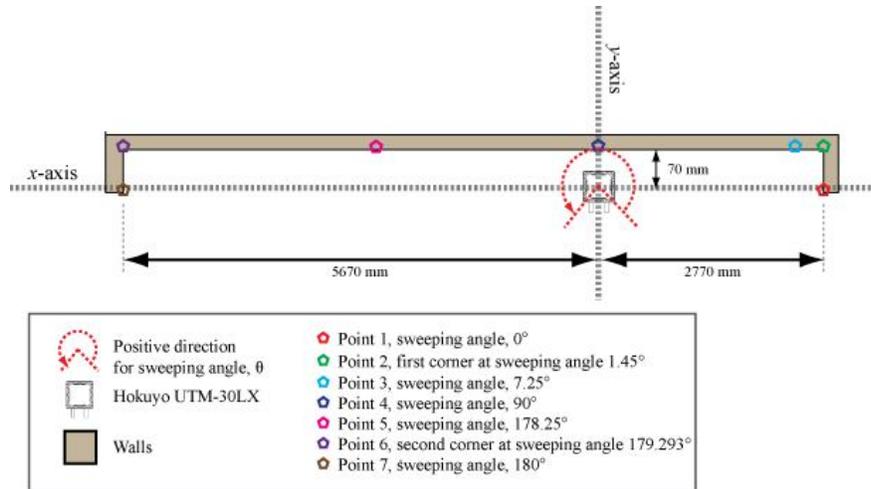
Fig. 10: Depiction of the controlled environment and its configuration consist of two right-angled corners and the points for kernel density estimation sampling and the actual setup of the experiment activity.
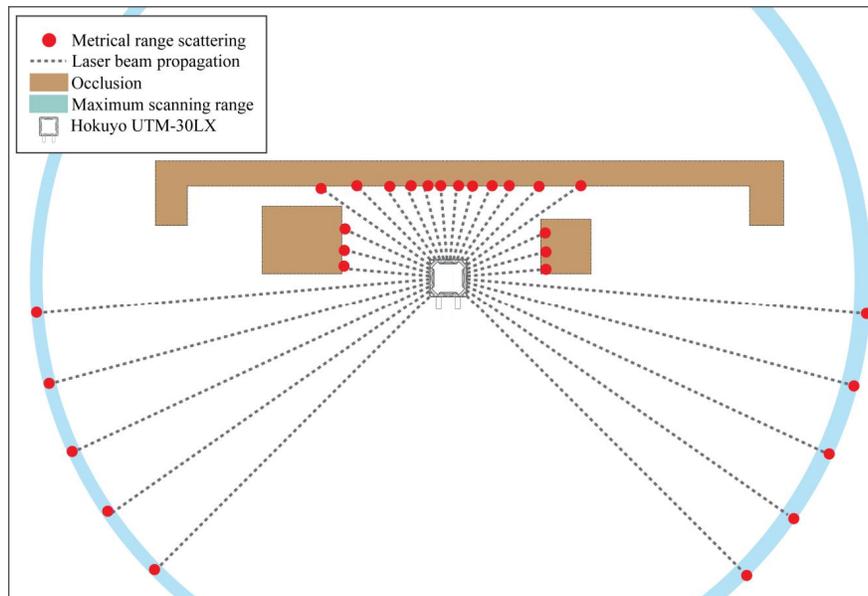
Fig. 11 The metrical range scattering is due to occlusion or propagation beyond the range of 30 m where the scanner would register *faux* occlusion at 30 m.

Instead of using one single range reading, this method mimics the real time application of the laser scanner by collecting 1000 scans of the controlled environment. This set up is chosen to push the boundary of the sensors response time and to give a good method to address the repeatability of a measurement with respect to response time. With 1000

iterations, the data that coincide with an expected value can be used to estimate the density of the reading.

The kernel density estimation is performed on 7 different points in the controlled environment of the experiment (Fig. 10). Each of these points has 1000 sets of data and the data are fed into kernel density estimation operator to find the underlying pattern which then be used to validate the Gaussian nature of the Hokuyo UTM-30LX reading. The estimated density are compared with an expected normal density based on the standard deviation of 10 mm [15].

5. RESULTS

5.1. Unimodal Estimated Density

All of the 1000 scans of the walls are superimposed into one point cloud which depicts the scattering of the range measurement range about the expected value of the wall. These metrical ranges have precision interval depicted in Fig. 12. The multiple isolated clusters noticeable in the left region of the metrical scatterings due to the 0.25^0 resolution of the planar sweep. The upper and lower boundary of the precision of the metrical range scatterings are calculated to show the overall precision of the metrical data collected.
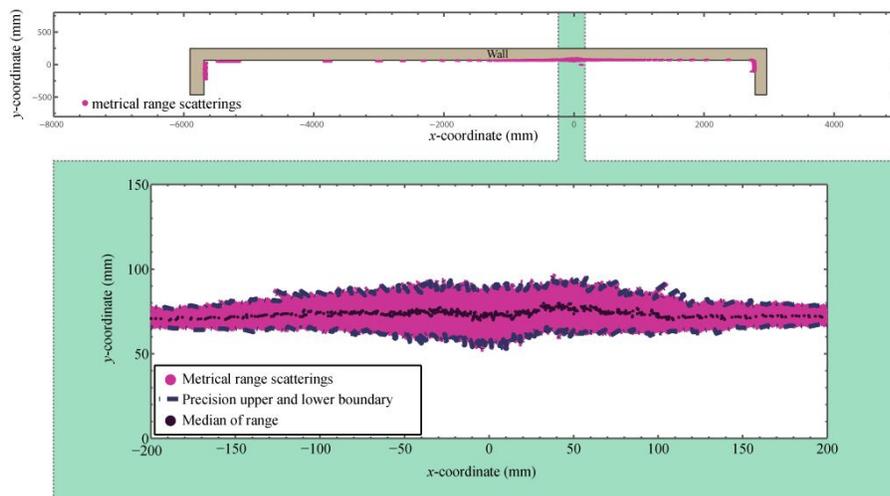
Fig. 12: The scattering of metrical range after 1000 scans in which the median, upper and lower boundary of the metrical range precision are computed from the kernel density estimation.

The standard deviation, median, and error for *Points 1* to *7* are calculated based on the density estimated from the kernel density estimation method. Table 1 summarizes these values. The error column in Table 1 is calculated based on the dimension of the wall seen in Fig. 10 and the median value is obtained from the estimated density. Table 1 gives insight of the highest error amongst the seven points of interest. This high error concludes that although the precision is high at *Point 5*, the accuracy of the reading are low due to high incident angle between the beam and the plane at that point. It is also observed that the precision of the metrical range decreases at the *second corner* at *Point 6* because of sharp edge at the position coupled with high incident angle. As the result of these factors, the error at *Point 6* is high at 216 mm. The standard deviations of all points are less than 10 mm with the exception of Point 6.

Table 1: Standard deviation, median, and error for metrical range at *Points 1* to *7*

Point	Standard deviation, σ (mm)	Median, µ (mm)	Error (mm)
1	5.020	2770	0.00
2	8.50	2729	42
3	7.96	568	11.50
4	4.93	73	2.48
5	8.47	2316	20
6	26.080	5317	216
7	6.57	5666	3

All the estimated density in *Points 1* to *7* are compared with expected normal density based on standard deviation, $\sigma_{expected}$=10 mm, about the actual range obtained from the dimensions of the experiment setup. The estimated density of *Points 1, 2, 3, 4, 7* are normal based on Figs. 14, 15, 16, 17, 18, and 20 respectively. However, the density estimated at *Point 6* shows skewing to the left about the median 5454 mm.
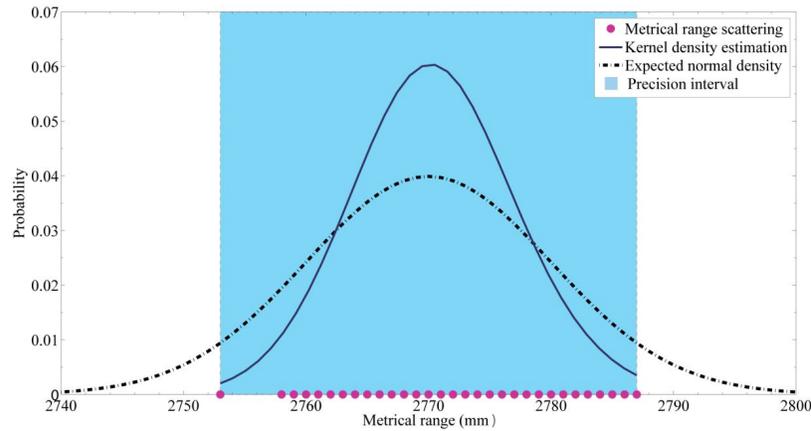
Fig. 13: Estimated density and normal density from *Point 1* with zero error.

Figure 13 shows a good example of a normal density with standard deviation smaller than the standard deviation of the expected normal density. The modality of the estimated density is unity and has no skewing.

In Fig. 14 the expected range is seen to be larger than the median of the estimated density. This does not affect the modality of the estimated density which is still unity with no local maxima. Such result is of interest since at *Point 2* the scanner encounters with the *first corner* in the wall. However, no tail or multimodality is seen in the estimated density at *Point 2*. The absence of density that could suggest multimodal density due to sharp edges might suggest that such anomaly only occurs at extreme incident angles. The only indication that a certain extreme feature encountered at *Point 2* from the metrical range data is the notable error.
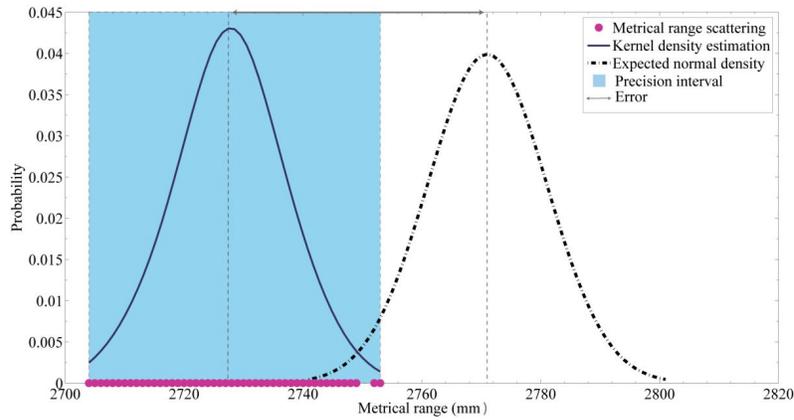
Fig. 14: Estimated density and normal density from *Point 2* with notable error of 42 mm.

Figure 15 presents the information of unimodality of the estimated density at *Point 3*. The estimated density is normal and almost symmetrical but with a small overshoot in median value. Figures 16, 17 and 18 present similar estimated densities at *Point 4*, *Point 5*, and *Point 7* respectively.
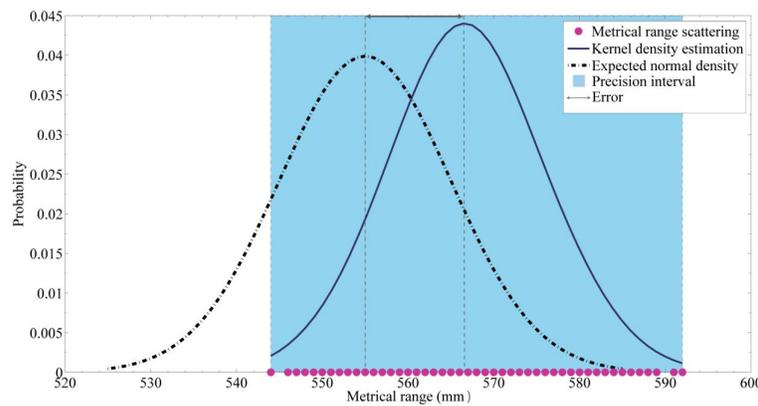
Fig. 15: Estimated density and normal density from *Point 3* with error of 11.5 mm.
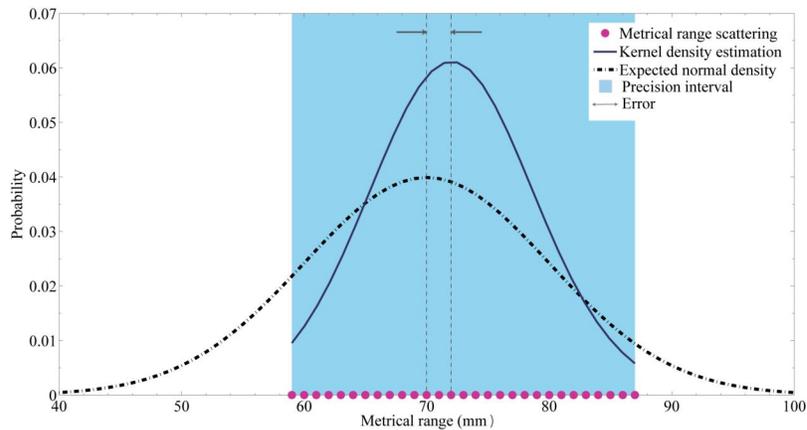
Fig. 16: Estimated density and normal density from *Point 4* with 2.48 mm of error.
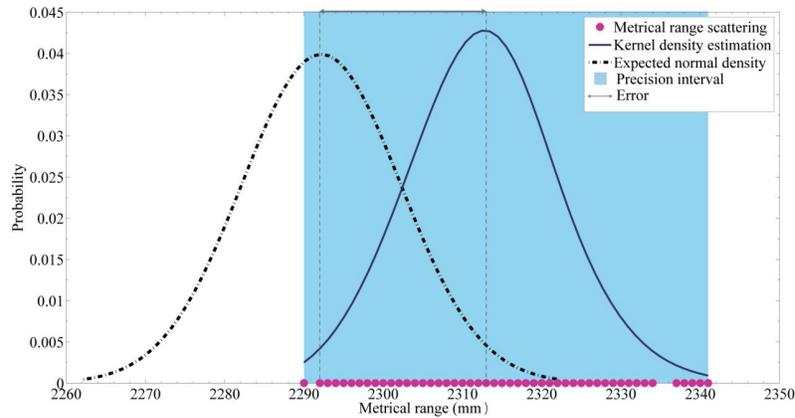
Fig. 17: Estimated density and normal density from *Point 5* with 20 mm error.
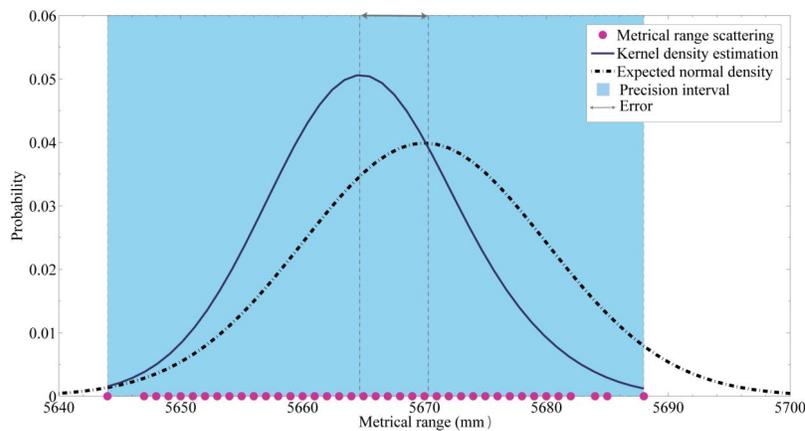
Fig. 18: Estimated density and normal density from *Point 7* with error of 3 mm.

5.2. Multimodal Density

The presence of two local maxima is observed from the density estimation at *Point 6*. The extreme angle change at the *second corner* causes the scattering of the metrical data to localize between two local maxima; 5454 mm and 5149 mm. The low number of scatterings at mode 5149 mm, however, has low probability. Instead, the density at mode 5454 mm skewed to the left due to scattering at mode 5149 mm. The corners on both *Point 2* and *Point 6* are similar but with different incident angle. Since the incident angle of the corner at *Point 6* is larger than that of *Point 2*, the effect of sharp edges due to corners are seen to have more effect on the density at *Point 6* than the density at *Point 2*. Figure 19 shows the estimated density of metrical data at *Point 6*.

Bimodal density is also observed for metrical data at angle sweep -2.25^{0}. Figure 20 shows two regions of local maxima, with *Region 2* having a density about mode 2766 mm (refer to Fig. 22), and *Region 1* having multimodal density (refer to Fig. 21). The scattering of the range between these two regions suggest that the scanner encounters a large discontinuity of reading, explained only by two occlusion separated at a large depth. This observation contradicts any reports or assumption that there is no effect of intermediate value between two occlusions separated by large depth [6]. Figure 23 explains the location of *Region 1* and *Region 2*.
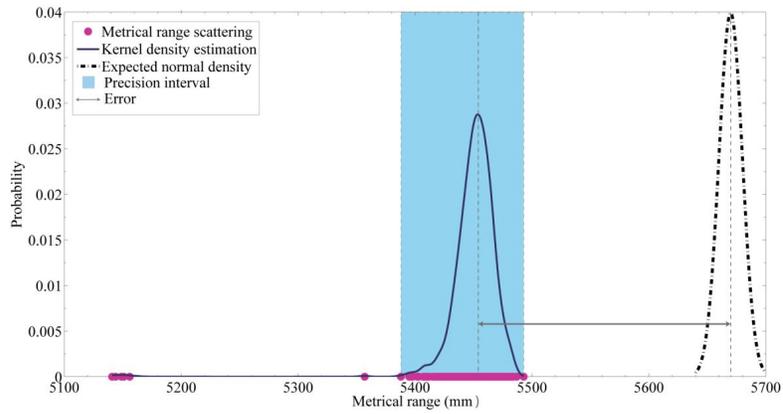
Fig. 19: Estimated density and normal density from *Point 6* with 216 mm error.
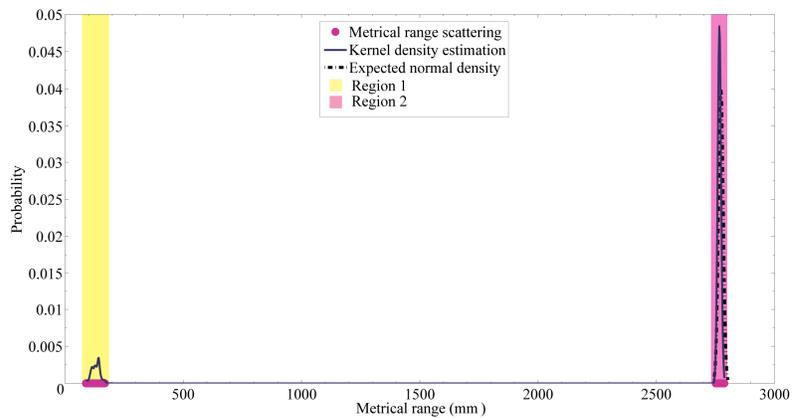
Fig. 20: Multiple modality at sweeping angle -2.25^0 are seen in *Region 1* and *Region 2*, due to the presence of two occlusions separated by a large depth, with higher frequency in *Region 1*.
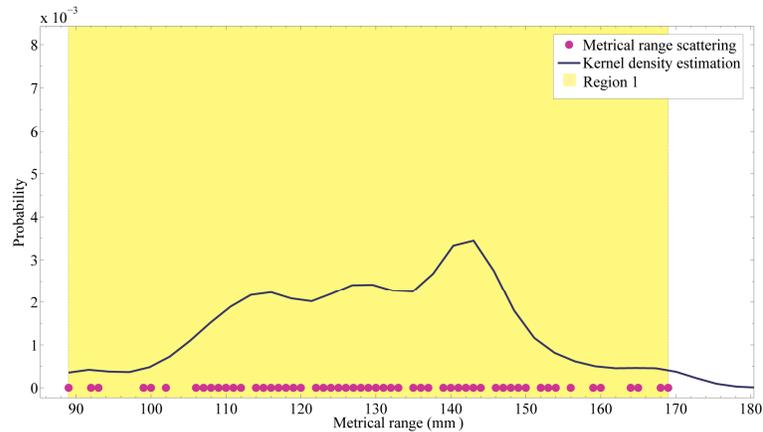
Fig. 21: Estimated density in *Region 1* with multimodal appearance of low probability.
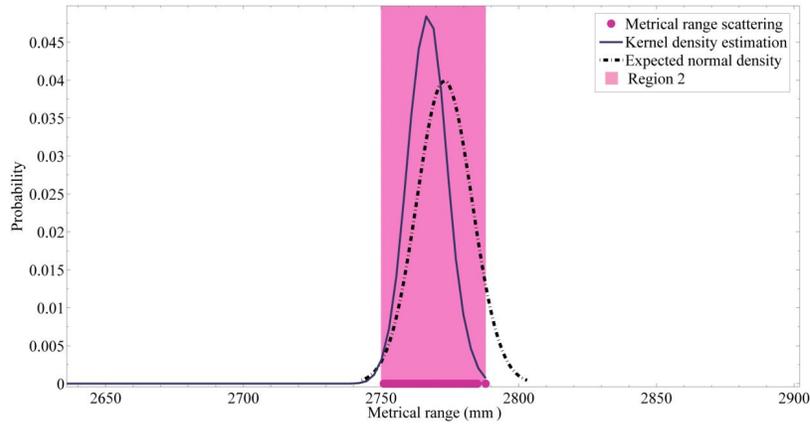
Fig. 22: Estimated density and expected density in *Region 2*.
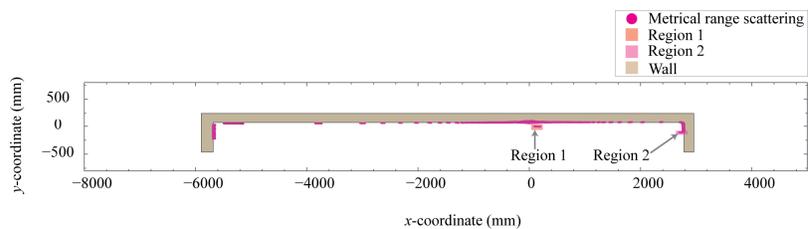
Fig. 23: Location of *Region 1* and *Region 2* in the metrical range scattering.

5.3. Standard Deviation, Error and Accuracy

The standard deviation of each incremental angle in the planar sweep is observed to change at 0.25^0 increments. The varying standard deviation is presented in Fig. 24. Figure 24 shows a high standard deviation in the discontinuity region at sweep angle -2.25^0. Also a faint spike of standard deviation is observed when the beam propagation traverses across *Point 2* where the *first corner* is encountered. This spike is also seen when the beam propagation of the laser traverses across *Point 6* where *second corner* is situated. The average standard deviation is 10.54 mm. The standard deviation value of 10.54 is used to map the controlled environment using voxelized grid cell mapping method. The map is depicted in Fig. 26 where each voxel was tessellated based on the value of the standard deviation.
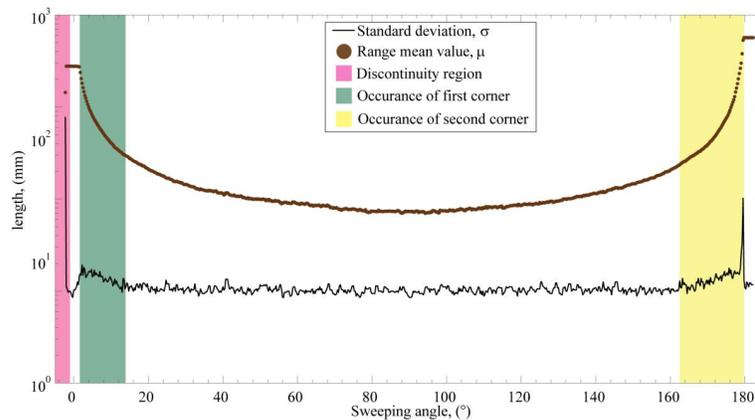
Fig. 24: Standard deviation for sweeping angle -2.25^0 to 182.25^0.

Two methods were used to find the error of each increment in the angle sweep. The naïve approach calculates the median based on the raw metrical data and compare the set of median values with the expected values. This results in a set of errors that is biased towards the maximum bound of the data reading. However, by using information from the estimated density, a more optimal set of error values can be calculated without any bias. Figure 25 includes the set of errors obtained from the naïve approach. The remaining discussion on error in this section will reflect error data from the latter approach.
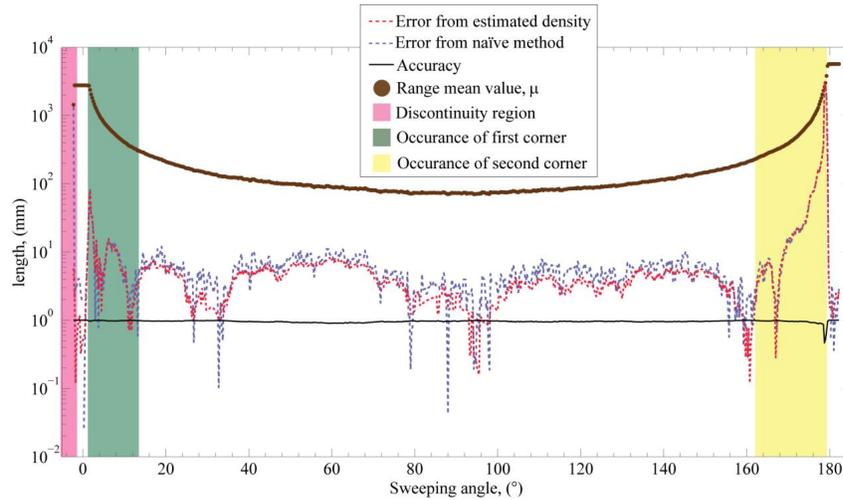
Fig. 25: Accuracy and error from sweeping angle -2.25^0 to 182.25^0.

The error on each angle sweep increment is observed to vary between 0 to 3039 mm. The large error margin is due to the nature of the environment that impose extreme angle of incident to the laser scanner. Unlike the value of standard deviation, the errors are nominal at discontinuity region of the controlled environment. Notwithstanding, high errors are seen at *Point 2* and *Point 6* where the beam propagation traverses into regions with corners. The accuracy of the laser range finder is high throughout the planar sweep but collapses when imposed with acute edges at high incident angles. The average accuracy of laser scanner under close-range confined environment is 0.96. Table 2 summarizes the result obtained.

Table 2: Summary on the behavior of the metrical data for Hokuyo UTM-30LX
under various conditions in closed-range environment

	Corners		Discontinuity
	High Incident Angle	**Low Incident Angle**	
Standard deviation	Increase	Increase	Increase at high rate
Error	High	High	Nominal
Accuracy	High	Low	High
Density of metrical data	Multimodal	Unimodal	Multimodal
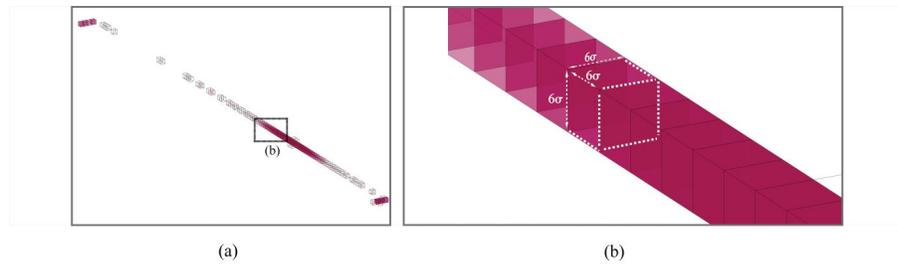
Fig. 26: Voxelized map of the control environment in the experiment protocol based on the value of standard deviation where (a) the map consist of tessellated grid cells with (b) length, width, and depth of each grid cells equal to 6*σ.

6. CONCLUSIONS

Under a confined close range environment, the Hokuyo UTM-30LX shows a slightly different behavior. The Standard deviation of the metrical data from the scanner increases while traversing through corners at incident angles approaching 90^0. Standard deviation also increases at a very high rate when the laser encounters discontinuity. The average standard deviation is 10.54 mm. The error reading is higher when the scanning traverses across corners but nominal for region with discontinuous depth. The error is even more pronounced for corners at incident angles approaching 90^0. The average accuracy of the sensor is high at 0.96. This accuracy is only affected if the laser is introduced to corners or sharp edges at incident angles between 85^0 and 90^0. The density of the metrical data throughout the planar sweeping is Gaussian in majority. Nevertheless, the normal density of the metrical data is affected when the scanning is imposed with discontinuity in depth. The collapse of the normal density is also seen when the scanning encounters corners at a high incident angle of 88.55^0 (*first corner*) to 89.29^0 (*second corner*). This information is crucial for the application of laser range finder in enclosed environments that introduce high incident angle such as SLAM for downstream pipes in oil and gas industry. The use of the method reported in this paper also optimized the value of the standard deviation of a laser scanner for use in any contingency in cluttered environment where extreme conditions such as close range scanning and high incident angles are likely to happen.

REFERENCES

[1]   Hebert M, Krotkov E. (1991) 3-D measurements from imaging laser radars: How good are they? in Intelligent Robots and Systems' 91: Intelligence for Mechanical Systems, Proceedings IROS'91. IEEE/RSJ International Workshop, pp. 359-364.
[2]   Thrun S. (2002) Probabilistic robotics. Commun. ACM, 45(3):52-57.
[3]   Silverman BW. (1986) Density estimation for statistics and data analysis. pp. 1-2.
[4]   Fernández-Madrigal JA. (2012) Simultaneous localization and mapping for mobile robots: introduction and methods. 1st edn., Hershey, PA, USA. IGI Global.
[5]   Ye C, Borenstein J. (2002) Characterization of a 2-D laser scanner for mobile robot obstacle negotiation. IEEE Int. Conf. on Robotics and Automation (ICRA), pp. 2512-2518.

[6]   Kneip L, Tache F, Caprari G, Siegwart R. (2009) Characterization of the compact Hokuyo URG-04LX 2D laser range scanner. IEEE Int. Conf. on Robotics and Automation (ICRA): pp. 1447-1454.

[7]   Alwan M, Wagner MB, Wasson G, Sheth P. (2005) Characterization of infrared range-finder PBS-03JN for 2-D mapping. IEEE Int. Conf. on Robotics and Automation (ICRA), pp. 3936-3941.

[8]   Pomerleau F, Breitenmoser A, Liu M, Colas F, Siegwart R. (2012) Noise characterization of depth sensors for surface inspections. 2nd International Conference in Applied Robotics for the Power Industry (CARPI), pp. 16-21.

[9]   Demski P, Mikulski M, Koteras R. (2013) Characterization of Hokuyo UTM-30LX laser range finder for an autonomous mobile robot. In Advanced Technologies for Intelligent Systems of National Border Security. Nawrat A, Simek K, Świerniak A., eds. Springer Berlin Heidelberg, 143-153.

[10]   Pouliot N, Richard P, Montambault S. (2012) LineScout power line robot: Characterization of a UTM-30LX LIDAR system for obstacle detection. IEEE/RSJ International Conference on Intelligent Robots and Systems (IROS), pp. 4327-4334.

[11]   Park CS, Kim D, You BJ, Oh SR. (2010) Characterization of the Hokuyo UBG-04LX-F01 2D laser rangefinder. 19th International Symposium in Robot and Human Interactive Communication, pp. 385-390.

[12]   Tretyakov V, Linder T. (2011) Range sensors evaluation under smoky conditions for robotics applications. IEEE International Symposium on Safety, Security, and Rescue Robotics (SSRR), pp. 215-220.

[13]   Shimazaki H, Shinomoto S. (2010) Kernel bandwidth optimization in spike rate estimation. J. Comput. Neurosci., 29(1-2):171-182.

[14]   Shimazaki H, Shinomoto S. (2007) A method for selecting the bin size of a time histogram. Neural Comput., 19(6):1503-1527.

[15]   Scanning range finder UTM-30LX | Photo sensor | PRODUCTS | HOKUYO AUTOMATIC CO.,LTD.”   [Online].   Available: https://www.hokuyo-aut.jp/02sensor/07scanner/utm_30lx.html. [Accessed: 21-Aug-2014].